

# Myosin-1c regulates the dynamic stability of E-cadherin-based cell–cell contacts in polarized Madin–Darby canine kidney cells

Hiroshi Tokuo and Lynne M. Coluccio

Department of Physiology and Biophysics, Boston University School of Medicine, Boston, MA 02118-2518

**ABSTRACT** Cooperation between cadherins and the actin cytoskeleton controls the formation and maintenance of cell–cell adhesions in epithelia. We find that the molecular motor protein myosin-1c (Myo1c) regulates the dynamic stability of E-cadherin-based cell–cell contacts. In Myo1c-depleted Madin–Darby canine kidney cells, E-cadherin localization was disorganized and lateral membranes appeared less vertical with convoluted edges versus control cells. In polarized monolayers, Myo1c-knockdown (KD) cells were more sensitive to reduced calcium concentration. Myo1c separated in the same plasma membrane fractions as E-cadherin, and Myo1c KD caused a significant reduction in the amount of E-cadherin recovered in one peak fraction. Expression of green fluorescent protein (GFP)–Myo1c mutants revealed that the phosphatidylinositol-4,5-bisphosphate-binding site is necessary for its localization to cell–cell adhesions, and fluorescence recovery after photobleaching assays with GFP–Myo1c mutants revealed that motor function was important for Myo1c dynamics at these sites. At 18°C, which inhibits vesicle recycling, Myo1c-KD cells accumulated more E-cadherin-positive vesicles in their cytoplasm, suggesting that Myo1c affects E-cadherin endocytosis. Studies with photoactivatable GFP–E-cadherin showed that Myo1c KD reduced the stability of E-cadherin at cell–cell adhesions. We conclude that Myo1c stabilizes E-cadherin at adherens junctions in polarized epithelial cells and that the motor function and ability of Myo1c to bind membrane are critical.

Monitoring Editor

Alpha Yap  
University of Queensland

Received: Dec 14, 2012

Revised: Jul 2, 2013

Accepted: Jul 2, 2013

## INTRODUCTION

Polarized epithelia, characterized by their distinct apical and basal surfaces, form boundaries between a specialized internal compartment and the external environment and are designed for the vectorial transport of ions and solutes. Polarized epithelia are formed in response to growth factors and their receptors, signaling pathways, and changes in gene expression when migratory cells aggregate and begin a complex series of events resulting in polarization

(Nelson, 2009). The polarized distribution of proteins is achieved by the sorting and targeting of exocytic vesicles from the Golgi complex to sites of growth on the apical or basolateral plasma membrane (Mostov *et al.*, 2000). In polarized epithelia, tight junctions (TJs; zonula occludens), adherens junctions (AJs; zonula adherens or adhesion belts), and desmosomes are localized at the juxtaluminal region and comprise the apical junctional complex (AJC; Farquhar and Palade, 1963). AJCs are located at the apex of the lateral membrane of polarized epithelial cells and regulate cell–cell adhesion, cell polarity, and paracellular permeability. They maintain the structural integrity of tissues and are formed by clustering of cell–adhesion proteins through binding between opposed extracellular domains; a portion of AJCs undergoes constant exchange and remodeling (Shen *et al.*, 2008).

During cell–cell junction formation cadherins cluster triggering rearrangement of the cytoskeleton and tethering of actin networks to the membrane (Cavey and Lecuit, 2009; Delva and Kowalczyk, 2009). Pharmacological agents that disrupt the actin cytoskeleton also disrupt cell–cell junctions. Cell–cell contact formation depends on actin assembly mediated by the Arp2/3 complex and formin-1,

This article was published online ahead of print in MBoC in Press (<http://www.molbiolcell.org/cgi/doi/10.1091/mbc.E12-12-0884>) on July 17, 2013.

Address correspondence to: Lynne M. Coluccio ([coluccio@bu.edu](mailto:coluccio@bu.edu)).

Abbreviations used: AJ, adherens junction; AJC, apical junctional complex; FN, fibronectin; FRAP, fluorescence recovery after photobleaching; GFP, green fluorescent protein; KD, knockdown; MDCK, Madin–Darby canine kidney; Myo, myosin; PAGFP, photoactivatable GFP; PH, pleckstrin homology; PIP<sub>2</sub>, phosphatidylinositol-4,5-bisphosphate; shRNA, short hairpin RNA; TJ, tight junction.

© 2013 Tokuo and Coluccio. This article is distributed by The American Society for Cell Biology under license from the author(s). Two months after publication it is available to the public under an Attribution–Noncommercial–Share Alike 3.0 Unported Creative Commons License (<http://creativecommons.org/licenses/by-nc-sa/3.0>).

“ASCB®,” “The American Society for Cell Biology®,” and “Molecular Biology of the Cell®” are registered trademarks of The American Society of Cell Biology.

which produces membrane protrusions, including lamellipodia and membrane ruffles, to initiate new contact sites (Braga *et al.*, 1999; Vasioukhin *et al.*, 2000; Bershadsky, 2004; Drees *et al.*, 2005; Ivanov *et al.*, 2005). Actin filaments both cluster cadherins and restrict their lateral movement at adherens junctions (Cavey *et al.*, 2008). The cytoplasmic tail of E-cadherin binds  $\beta$ -catenin, which binds  $\alpha$ -catenin (Bershadsky, 2004; Yonemura *et al.*, 2010).  $\alpha$ -Catenin couples the cadherin–catenin complex to actin (Kametani and Takeichi, 2007; Cavey *et al.*, 2008); however, the association of  $\alpha$ -catenin with actin might also be through other actin-binding proteins, such as vinculin,  $\alpha$ -actinin, formin, ZO-1, afadin, and epithelial protein lost in neoplasm (EPLIN), which bind  $\alpha$ -catenin (Harris and Tepass, 2010).

Actin-based motors are also implicated in cadherin biology. Five classes of myosins—myosins I, II, VI, VII, and X—are known to mediate cadherin-based cell–cell adhesion. Myosin-IId (Myo1d) directly binds  $\beta$ -catenin at adherens junctions to control left–right asymmetry in *Drosophila* (Speder *et al.*, 2006; Petzoldt *et al.*, 2012). Mice in which myosin II is ablated show defects in cell adhesion attributable to loss of E-cadherin and  $\beta$ -catenin at cell adhesion sites (Conti *et al.*, 2004; Shewan *et al.*, 2005; Applewhite *et al.*, 2007). Different myosin II isoforms have distinct roles at adherens junctions, with myosin IIa promoting E-cadherin adhesion and clustering and myosin IIb supporting the integrity of the apical cortical actin ring (Smutny *et al.*, 2010). In *Drosophila* myosin VI is required for border cell migration by stabilizing E-cadherin and armadillo ( $\beta$ -catenin; Geisbrecht and Montell, 2002), and in mammalian cells myosin VI is involved in the AP-1B–dependent sorting of proteins to the basolateral plasma membrane in the polarized epithelial cell line Madin–Darby canine kidney (MDCK; Au *et al.*, 2007). In addition, myosin VI is recruited to E-cadherin adhesions, mediates vinculin and E-cadherin interactions at cell–cell contacts, and is important for the integrity of adherens junctions (Maddugoda *et al.*, 2007). Myosin VII is required for normal adhesion of the leading edge of migrating *Dictyostelium* amoebae to the substrate and cell–cell adhesion (Tuxworth *et al.*, 2001). Myosin X transports VE-cadherin along filopodia to form early endothelial cell–cell contacts (Almagro *et al.*, 2010).

Class I myosins are the most diverse members of the myosin superfamily, and vertebrates express eight isoforms (Myo1a–h; Coluccio, 2008). Myo1c is widely distributed in vertebrate tissues. Its single 110-kDa heavy chain consists of a motor domain, three calmodulin-binding (IQ) domains, and a tail domain with a putative pleckstrin homology (PH) domain, which interacts with the phosphoinositides phosphatidylinositol-4,5-bisphosphate (PIP<sub>2</sub>) and phosphatidylinositol-3,4,5-trisphosphate (Hirono *et al.*, 2004; Hokanson *et al.*, 2006). It has been proposed that myosin I acts as a molecular force sensor, resulting in its conversion from low- to high-duty-ratio motor (Geeves *et al.*, 2000; Batters *et al.*, 2004a,b; Laakso *et al.*, 2008). The rate of Myo1c detachment from actin decreases significantly at forces of >1 pN (Greenberg *et al.*, 2012). In cells, myosin I makes a major contribution to membrane tension (Nambiar *et al.*, 2009).

In adipocytes Myo1c interacts with the small GTPase RalA and plays a role in the cycling of GLUT4-containing vesicles by promoting vesicle fusion with the plasma membrane via the exocyst (Bose *et al.*, 2002, 2004; Chen *et al.*, 2007). In the specialized hair cells of the inner ear Myo1c is associated with the electron-dense regions of the stereocilia, where the upper extracellular tip links insert into the stereociliary membrane (Gillespie and Müller, 2009). The current model for mechanotransduction is one in which Myo1c regulates the tension on these tip links, which connect neighboring stereocilia and control the opening and closing of

mechanically sensitive transduction channels (Gillespie and Müller, 2009). In the kidney, Myo1c is associated with podocytes in the glomerulus (Arif *et al.*, 2011), is present in most, if not all, tubule segments, including collecting tubules, and is found in the brush border of PT cells (Wagner and Molitoris, 1997; Boyd-White *et al.*, 2001). In collecting ducts Myo1c participates in the regulation of Na<sup>+</sup> channels after antidiuretic hormone stimulation (Wagner *et al.*, 2005).

Myo1c localizes to actin-rich regions at the periphery of tissue culture cells and in discrete punctae within the cytoplasm (Wagner *et al.*, 1992; Wagner and Molitoris, 1997; Ruppert *et al.*, 1995; Hokanson *et al.*, 2006). It cofractionates with several membrane fractions, including plasma membrane and endosomes from liver (Ruppert *et al.*, 1995; Balish *et al.*, 1999). Myo1c is reportedly involved in the late endocytic pathway, which delivers endocytosed macromolecules to lysosomes for degradation (Poupon *et al.*, 2003; Walmsley *et al.*, 2010), whereas new evidence associates Myo1c with the delivery of lipid-raft membranes to the cell surface (Brandstaetter *et al.*, 2012).

In this study we investigate the role of Myo1c in MDCK epithelial cells by RNA interference. Cells expressing reduced levels of Myo1c exhibit a flattened phenotype in low-density culture. At high density, the phenotype of the polarized epithelia is relatively normal but more sensitive to lower Ca<sup>2+</sup> concentrations, which cause detachment. Only wild-type Myo1c rescues the Myo1c-knockdown (KD) phenotype. Myo1c KD does not affect E-cadherin expression, but cell attachment to the E-cadherin ectodomain decreases and the stability of E-cadherin at cell–cell adhesions is reduced. These findings suggest that Myo1c motor activity and membrane binding play roles in the maintenance of E-cadherin–mediated adherens junctions in polarized epithelial cells.

## RESULTS

### Localization of Myo1c at sites of cell–cell contact

When polarized MDCK cells were stained for Myo1c, considerable staining was observed at sites of cell–cell contact (Figure 1A). These same areas were positive for E-cadherin, a major component of adherens junctions. Image analysis showed that Myo1c and E-cadherin colocalized (Figure 1B).

### Gene silencing of Myo1c in MDCK cells

To investigate the role of Myo1c in cell–cell contact, we selected several target sequences from the canine Myo1c gene and used them to construct pSUPER vectors for the expression of small hairpin RNAs (shRNAs). Two of the shRNAs efficiently knocked down Myo1c expression when expressed by transient transfection in MDCK cells. To obtain cells in which Myo1c expression is continually knocked down, we selected clones expressing these shRNAs. Multiple cell lines were characterized to control for clonal variation, and two representative lines (Myo1cKD1, Myo1cKD2) were chosen for further experiments (Figure 2A).

Immunofluorescence microscopy revealed that Myo1c was associated with lateral plasma membranes at sites of cell–cell adhesion, and staining was substantially reduced in the KD cells (Figure 2B). When normal MDCK cells were cultured at low density, they organized into discrete, tight islands with smooth boundaries, but cells with reduced amounts of Myo1c appeared more fibroblastic (Figure 2C). They spread and flattened and exhibited more stress fibers than control cells when stained with phalloidin (Figure 2B). These observations suggested that Myo1c might regulate epithelial cell–cell adhesion.

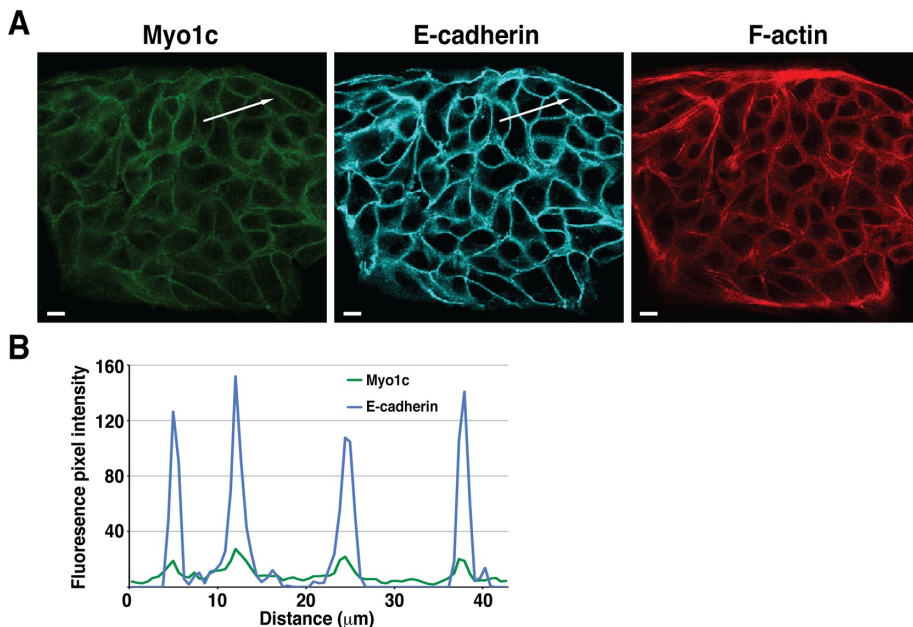


**FIGURE 1:** Myo1c colocalizes with E-cadherin at regions of cell–cell contact. (A) Representative confocal image of MDCK cells stained with anti-Myo1c (Myo1c), anti-E-cadherin antibodies (E-cadherin), the appropriate secondary antibodies, and rhodamine–phalloidin to visualize actin (F-actin). (B) Line-scanning analysis of fluorescence intensity at the region indicated by the arrows in A was used to quantitate the Myo1c and E-cadherin content. Scale bars, 10  $\mu\text{m}$ .

### Depletion of Myo1c causes a defect in cell–cell adhesive junctions

To further elucidate the function of Myo1c in epithelial cell–cell adhesion, we examined the distribution of E-cadherin and ZO-1 in Myo1c-KD cells. In control cells, these proteins colocalized along the lateral cell boundaries (Figure 3A). Myo1c KD caused a distinctive phenotype in which the lateral membranes of the cells became disorganized, appearing less vertical and with convoluted edges (Figure 3A). Similarly, E-cadherin localization in the KD cells was

disorganized as compared with control cells. ZO-1 was still localized all around the cell–cell adhesion sites between the Myo1c-KD cells (Figure 3B). The total amounts of ZO-1, E-cadherin,  $\beta$ -catenin, and occludin in the KD cells were the same as in control cells (Figure 3C); therefore Myo1c does not regulate the expression of these junctional proteins.

### Myo1c is required for E-cadherin–mediated adhesion

To determine whether the defect in cell–cell adhesion in Myo1c-KD cells is mediated through E-cadherin or some other cell adhesion protein, we assayed the ability of MDCK cells to attach to E-cadherin. Cells were dissociated using an ethylene glycol tetraacetic acid solution (without trypsin), collected, and resuspended in fresh medium, then plated in the presence of arginine–glycine–aspartic acid peptide, which blocks integrin-mediated attachment, on a 96-well plate coated with the recombinant ectodomain of human E-cadherin fused to the Fc region of immunoglobulin G (Qin et al., 2005). After cells were allowed to attach for 60 min, the

plates were washed and the remaining cells were counted. As shown in Figure 4, almost no cells attached to the plates in the absence of E-cadherin ectodomain. In the presence of the E-cadherin ectodomain, control cells attached efficiently, and attachment was proportional to the amount of E-cadherin ectodomain coating the plates (Figure 4). Loss of Myo1c caused substantial decrease (approximately threefold) in cell attachment, demonstrating that E-cadherin homophilic adhesion was compromised in the absence of Myo1c.

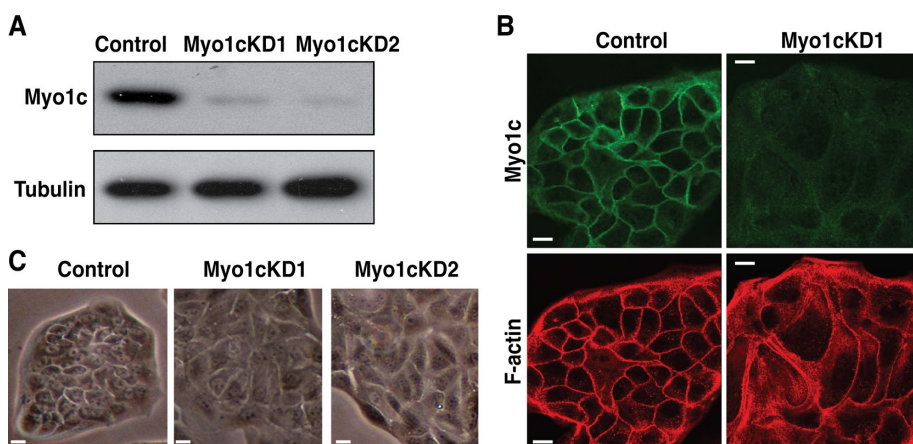


**FIGURE 2:** Suppression of Myo1c expression results in loss of epithelial morphology of MDCK cells at low density. (A) MDCK cells were transfected with either pSUPER-luciferase vector (Control) or one of two pSUPER constructs targeting different sequences of canine Myo1c mRNA (Myo1cKD1, Myo1cKD2), and stable cell lines were selected. Equal amounts of proteins were analyzed by SDS–PAGE and immunoblotting using the signal from anti-tubulin antibody as a loading control. (B) Control and Myo1c-KD cells were grown at low density for 3 d, fixed, and stained with anti-Myo1c antibodies to visualize Myo1c and rhodamine phalloidin to visualize F-actin. (C) Images of live control and Myo1c-KD cells were obtained by phase-contrast microscopy using a 10 $\times$  objective lens. Scale bars, 10  $\mu\text{m}$ .

### Myo1c is required for maintenance of an epithelial phenotype regulated by $\text{Ca}^{2+}$

To investigate further the potential role of Myo1c in cell–cell adhesion, we attempted classic calcium switch experiments; however, many Myo1c-KD cells detached after culturing overnight in MEM lacking  $\text{Ca}^{2+}$  and supplemented with 2% dialyzed fetal bovine serum (FBS). Instead, we investigated the effect of different  $\text{Ca}^{2+}$  concentrations on cell–cell adhesion under high-density culture conditions. After 6 d of culturing with growth medium (GM), both control and Myo1c-KD cells developed vertical lateral boundaries and a highly packed phenotype, as observed with phalloidin staining of z-sections and middle sections, although the bottom section showed a striking difference (Supplemental Figure S1). At the bottom, control cells exhibited few stress fibers, but Myo1c-KD cells had thick stress fibers. Little change in E-cadherin staining was observed between control and KD cells in GM

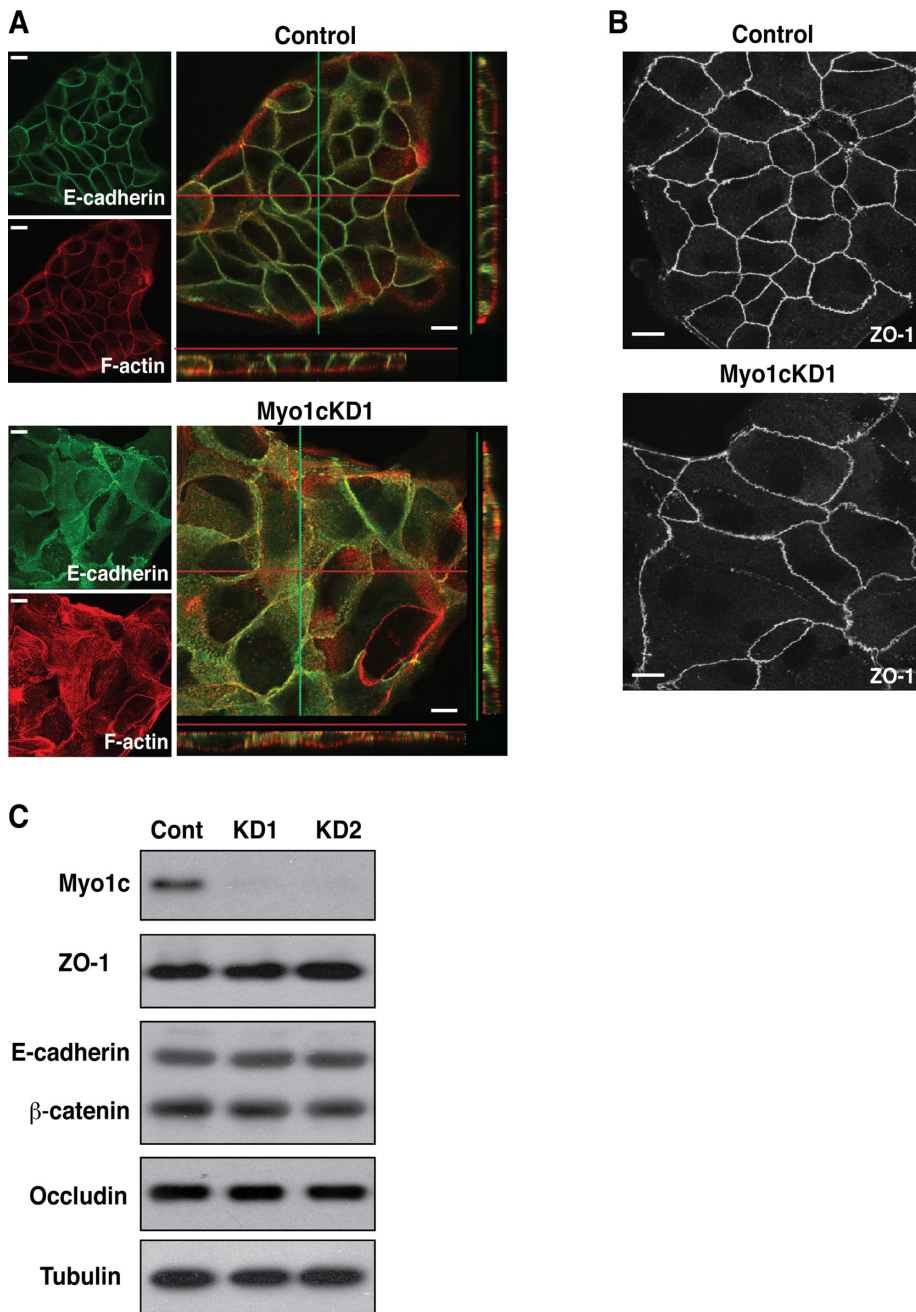


**FIGURE 3:** Loss of Myo1c causes a defect in cell–cell adhesive junctions. (A) Control and Myo1c-KD cells were plated at low density and then fixed and stained for E-cadherin (green) and F-actin (red). Image stacks were collected using confocal microscopy with 0.9- $\mu$ m z-steps. (B) Control and Myo1c-KD cells were stained for ZO-1. Scale bars, 10  $\mu$ m. (C) Immunoblot of junctional proteins in control and Myo1c-KD cells. Whole-cell lysates were blotted for Myo1c, ZO-1, E-cadherin,  $\beta$ -catenin, occludin, and tubulin.

(Supplemental Figure S1). After reduction of the calcium concentration to 50  $\mu$ M for 4 h (Figure 5, A–D), control cells still showed intact cell–cell adhesions with E-cadherin staining, but Myo1c-KD cells started to detach from each other and showed diffuse E-cadherin staining.

To quantify the changes in E-cadherin morphology, we performed line scan analysis of fluorescence intensity at cell–cell contacts (Supplemental Figure S2). Nonlinear fit curves of contact profiles in control and Myo1c-KD cells were acquired (Figure 5E). The lateral distribution of E-cadherin from the cell–cell contact in

Myo1c-KD cells was larger than that in control cells, as measured by the average of the width (Figure 5F; control,  $0.8 \pm 0.05 \mu$ m; Myo1c KD,  $1.7 \pm 0.2 \mu$ m) and the average peak fluorescence intensity (Figure 5C; control,  $127 \pm 10$ ; Myo1c KD,  $81 \pm 9$ ) for each contact profile. At 5 and 0  $\mu$ M  $\text{Ca}^{2+}$  (Supplemental Figure S1), control cells started to detach from each other, but staining of E-cadherin was still evident, and ring-like actin structures at the bottom indicated cell–substrate adhesion. On the other hand, Myo1c-KD cells showed reduced cell–cell attachment at these lower  $\text{Ca}^{2+}$  concentrations, with diminished actin staining at the bottom. Furthermore, in control cells localization of Myo1c also dynamically changed as a function of  $\text{Ca}^{2+}$  concentration and colocalized with E-cadherin, especially at the middle section (Supplemental Figure S1C). These observations suggest that Myo1c might function to maintain AJs even in low- $\text{Ca}^{2+}$  conditions.

### Cofractionation of AJCs with Myo1c

To investigate in more detail the localization and function of Myo1c at the basolateral membrane, we examined different plasma membrane domains separated by centrifugation in iodixanol gradients for the presence of Myo1c and components involved in cell–cell adhesion. Control and Myo1c-KD cells were homogenized 48 h after induction of cell–cell adhesion, and the homogenates were fractionated in 10–30% Opti-Prep gradients. The distributions of Myo1c, E-cadherin,  $\beta$ -catenin, ZO-1, occludin, and the exocyst component Sec8 were determined by SDS–PAGE and immunoblotting (Figure 6). Myo1c was found predominantly in three membrane fractions with respective peak densities of 1.10, 1.12, and 1.16 g/ml (Figure 6A). E-cadherin and  $\beta$ -catenin were mainly recovered in these same three fractions and an additional fraction with density of 1.20 g/ml. In Myo1c-KD cells, substantially less E-cadherin and  $\beta$ -catenin were recovered in the membrane fraction, with the density of 1.10 g/ml (Figure 6B). This peak was shown to contain non-junction-associated basolateral membranes (Yeaman, 2003). Basolateral-specific proteins were recovered in the peaks at both 1.16 and 1.10 g/ml; therefore these gradients appear to resolve subdomains of basolateral membrane fractions containing intercellular junctions ( $\sim$ 1.16 g/ml) and non-junction-associated membranes ( $\sim$ 1.10 g/ml) (Yeaman, 2003). The tight junction protein ZO-1 was distributed in control cells in a peak fraction with density of 1.12 g/ml and fractions with densities between 1.18 and 1.20 g/ml. The peak fraction of ZO-1 was reduced in Myo1c-KD cells. Another tight junction protein, occludin, was sedimented in two membrane fractions with peak densities of 1.10 and 1.12 g/ml in control cells. In Myo1c-KD cells, the peak fraction

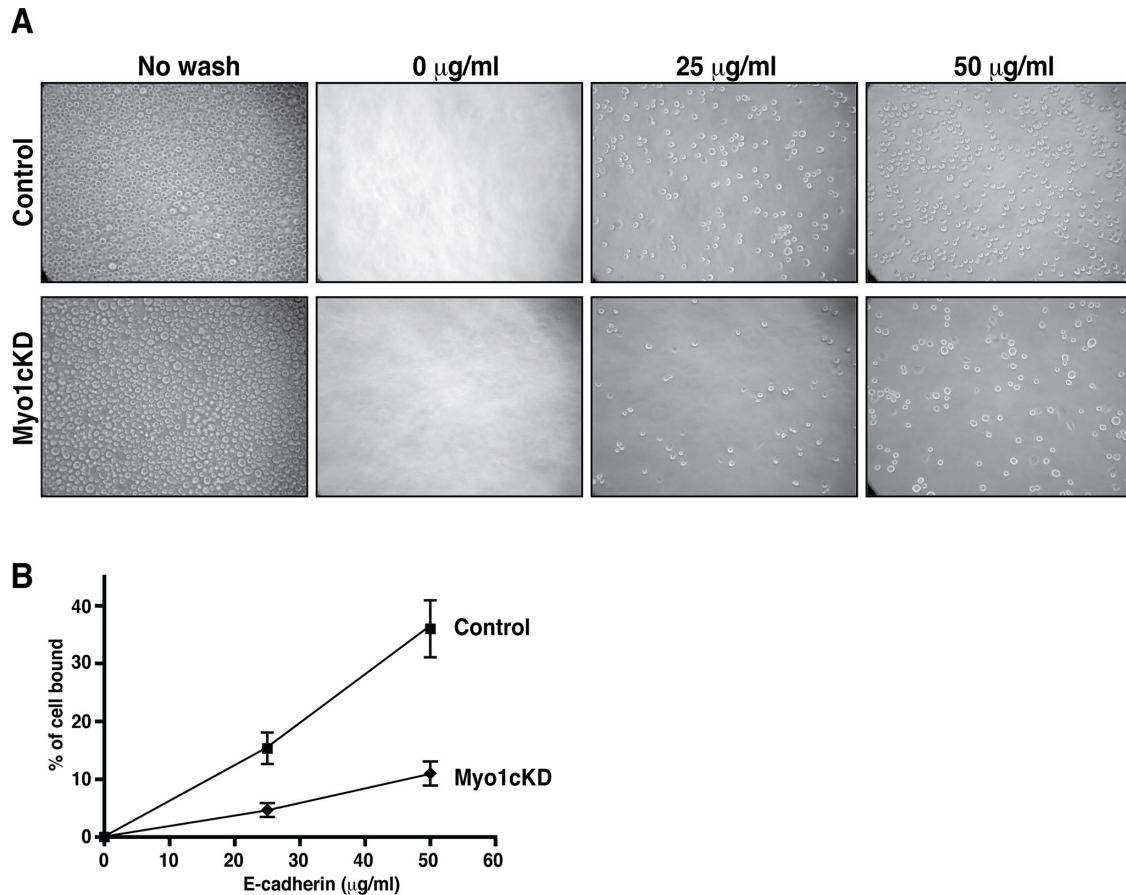


**FIGURE 4:** Suppression of Myo1c reduces E-cadherin-mediated adhesion. (A) Control and Myo1c-KD cells were allowed to adhere for 60 min to plates coated with different concentrations of recombinant E-cadherin ectodomain. Unattached cells were washed out, and images were captured. (B) Quantification of cell attachment to E-cadherin ectodomain. The number of cells on unwashed plates was used to calculate the total number of cells (100%). Data represent the means  $\pm$  SD of 15 images from triplicates of each condition.

of occludin at 1.10 g/ml was reduced. Sec8 was recovered in the same fractions as ZO-1 in control cells, but in Myo1c-KD cells, Sec8 was found predominantly in fractions with densities of 1.12 and 1.16 g/ml. These fractionation patterns suggest that Myo1c might be more associated with AJ complexes than TJ complexes. To address this issue, we performed immunoprecipitation assays. Myo1c precipitated with anti-Myo1c antibody, but neither E-cadherin,  $\beta$ -catenin, ZO-1, nor Sec8 was detected even after cross-linking with a cell-permeable cross-linker before cell lysis (data not shown). These results suggest that either Myo1c does not directly associate with AJCs or the association is not strong enough to be detected by immunoprecipitation assays.

#### Myo1c domains responsible for its localization at cell-cell adhesions

To examine which functional domains and/or amino acids in Myo1c are responsible for its localization to sites of cell-cell contact, we constructed a series of green fluorescent protein (GFP)-Myo1c expression vectors containing point mutation or those in which specific domains (motor, IQ, or tail) were deleted (Figure 7A). Their effects on localization were observed in polarized MDCK cells (Figure 7B). Deletion of the tail domain (Myo1c-MoIQ2) blocked the accumulation of GFP-Myo1c at cell-cell adhesions, but deletion of the motor domain (Myo1c-IQT) or motor and IQ domains (Myo1c-T) did not affect

localization at cell-cell contacts. These results suggest that accumulation of Myo1c at cell-cell adhesions depends on the tail domain but not on the motor and IQ domains. For additional evidence that motor activity is not required, we prepared constructs with mutations in the switch I (R162A) or switch II (G389A) region of the motor domain of GFP-Myo1c, which render the molecule inactive or motor dead. The amino acid sequence of the switch I loop (NXNSSRFG; residues 157–164) is conserved in almost all myosins sequenced, including Myo1c (Shimada *et al.*, 1997). The R-to-A mutation in switch I results in loss of ATP binding in skeletal muscle myosin-II (Li *et al.*, 1998). Additional studies with *Dictyostelium* myosin II show that the mutation results in a myosin in the weak-binding state and unable to support actin-filament sliding in vitro (Shimada *et al.*, 1997).

The motor domain of Myo1c also contains the conserved sequence of the switch II loop (DIYGFE; except that F is in the third position). Switch II interacts with the switch I loop, and this interaction is critical for ATP hydrolysis by myosin (Li *et al.*, 1998). Although the G-to-A mutation in switch II does not abolish binding of ATP to the active site, ATP hydrolysis is inhibited, myosin is held in the weak-binding state, and no actin is translocated in motility assays (Sasaki *et al.*, 1998; Kambara *et al.*, 1999). When expressed in MDCK cells, these two mutations did not inhibit the localization of GFP-Myo1c at cell-cell adhesions (Figure 7B), evidence that Myo1c localization does not require motor activity.

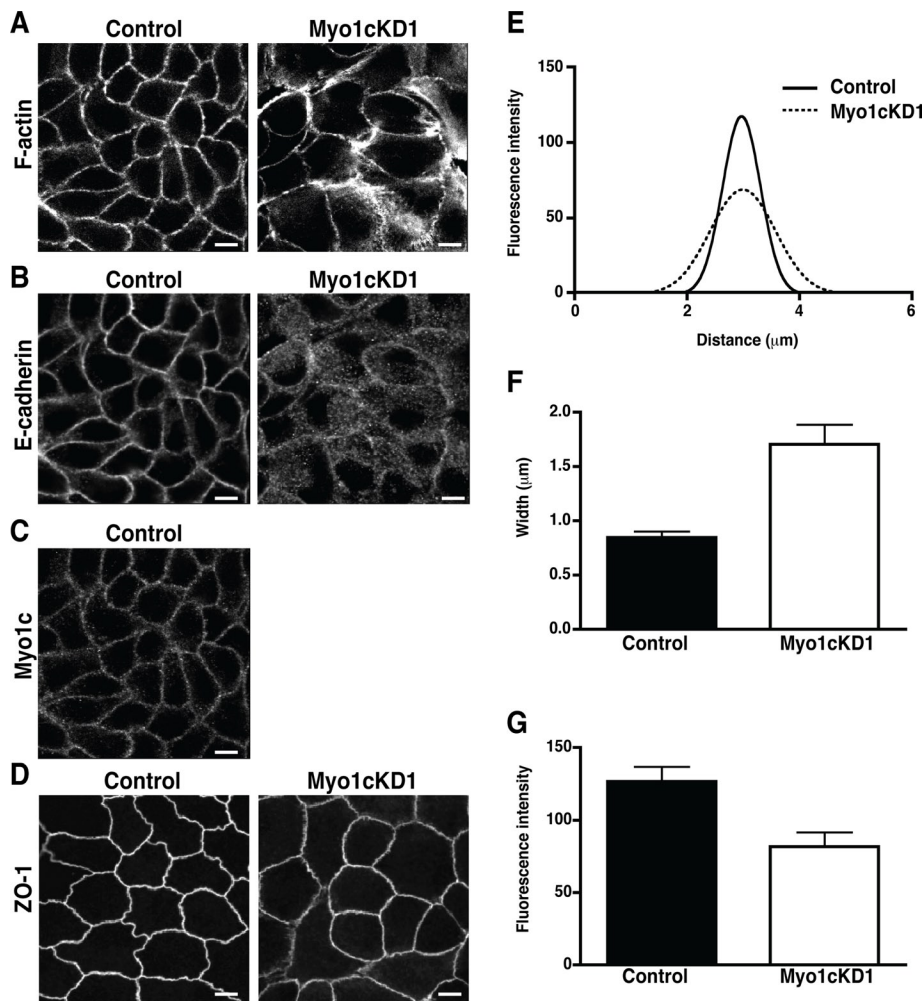


**FIGURE 5:** Suppression of Myo1c increases the sensitivity of cell–cell contacts to  $\text{Ca}^{2+}$ . Control and Myo1c-KD cells were plated at high density for 3 d and then incubated in media containing 50  $\mu\text{M}$   $\text{Ca}^{2+}$  for 4 h. Cells incubated with a series of different  $\text{Ca}^{2+}$  concentrations (0  $\mu\text{M}$  to GM) are shown in Supplemental Figure S1. Fixed cells were stained for F-actin (A), E-cadherin (B), Myo1c (C), and ZO-1 (D). Image stacks were collected using confocal microscopy with 0.9- $\mu\text{m}$  z-steps. (E–G) Changes in E-cadherin distribution at cell–cell contacts were quantified by line-scan analysis of fluorescence intensity. (E) Nonlinear fit curves of contact profiles in control and Myo1c-KD cells ( $n = 24$ ). Contact profiles with means and SD are shown in Supplemental Figure S2. (F) The average width of E-cadherin in control and Myo1c-KD cells. Data are mean and SEM. (G) Average peak fluorescence intensity values of E-cadherin in control and Myo1c-KD cells. Data are mean and SEM.

Myo1c has a putative PH domain in its tail region and binds  $\text{PIP}_2$  (Hokanson *et al.*, 2006; Hokanson and Ostap, 2006). Mutation of basic residues in the signature motif of the PH domain (K892A or R903A) inhibits binding to  $\text{PIP}_2$  and localization within membrane ruffles (Hokanson *et al.*, 2006). We used these same mutations in GFP-Myo1c to investigate whether Myo1c localization at cell–cell adhesions depends on  $\text{PIP}_2$  binding. As shown in Figure 7B, both mutations completely inhibited targeting of Myo1c to cell–cell contacts; instead, these proteins accumulated in the cytoplasm. Together these results indicate that Myo1c localization at cell–cell adhesions depends on its tail domain, especially the  $\text{PIP}_2$ -binding sites, whereas the motor domain and motor function are not required.

#### Dynamic exchange of Myo1c at cell–cell adhesions

AJCs are dynamically exchanged and remodeled at steady state (Shen *et al.*, 2008). To investigate the stability of Myo1c at cell–cell

adhesions, we measured its dynamics in live confluent MDCK monolayers using fluorescence recovery after photobleaching (FRAP; Figure 7). Regions within the junctions between two adjacent transfected cells were selected for bleaching (white box in Figure 7C), and the average intensity was monitored during recovery. The majority of Myo1c associated with cell–cell adhesions was available for exchange; the mobile fraction was 70.7% (Figure 7, C and D). (Raw data of FRAP and average fluorescence intensity profiles are shown in Supplemental Figure S1.) This exchange occurred rapidly with a 7.3-s half-time of fluorescence recovery ( $t_{1/2}$ ).

To assess the mechanism of this dynamic behavior of Myo1c, we measured FRAP for the truncation mutant GFP-Myo1cIQT and the motor-domain mutants GFP-Myo1cR162A and GFP-Myo1cG389A. Of interest, absence of the motor domain (GFP-Myo1cIQT) increased the mobile fraction to 79.3% ( $p < 0.0001$ ; Student's  $t$  test) with faster recovery ( $t_{1/2} = 5.6$  s,  $p < 0.001$ ). The faster recovery of Myo1cIQT versus full-length Myo1c might be due to the inability of Myo1cIQT to bind to cortical actin filaments, such that its localization at the membrane is a consequence only of phospholipid binding, which is dictated by the putative PH domain in the tail region (Hokanson *et al.*, 2006; Hokanson and Ostap, 2006). In the case of the two motor-dead mutants (R162A, G389A), the G389A mutation decreased the mobile fraction to 61.5% ( $p < 0.001$ ), but the R162A mutation did not affect it. Both mutants showed a slower rate of recovery than wild-type Myo1c (R162A, 13.6 s,  $p < 0.0001$ ; G389A, 17.7 s,  $p < 0.0001$ ). Both mutations affect the motor activity, with mutations in switch I having a defect in ATP hydrolysis (Shimada *et al.*, 1997) and mutations in switch II affecting the isomerization step of the ATPase cycle (Sasaki *et al.*, 1998); the lack of ATPase activity

results in weak binding of myosin to actin (Shimada *et al.*, 1997; Sasaki *et al.*, 1998). The slower fluorescence recovery observed with these mutants after bleaching indicates that nucleotide cycling contributes to Myo1c localization at the membrane. Together these results demonstrate that the mobility of Myo1c at cell–cell contacts is partially dependent on its motor domain and motor function. It is plausible that the interaction of the Myo1c motor domain with actin increases its stability at cell–cell adhesion sites.

#### Knockdown of Myo1c does not affect actin dynamics at cell–cell contacts

Actin is highly dynamic at cell–cell contacts, as evidenced by FRAP studies showing that 90% of GFP-actin is mobile, with  $t_{1/2} = 9.6$  s (Yamada *et al.*, 2005). To study further the relationship between Myo1c and actin at cell–cell adhesions, we investigated the effect of Myo1c KD on FRAP of GFP-actin. Junctional actin recovery was

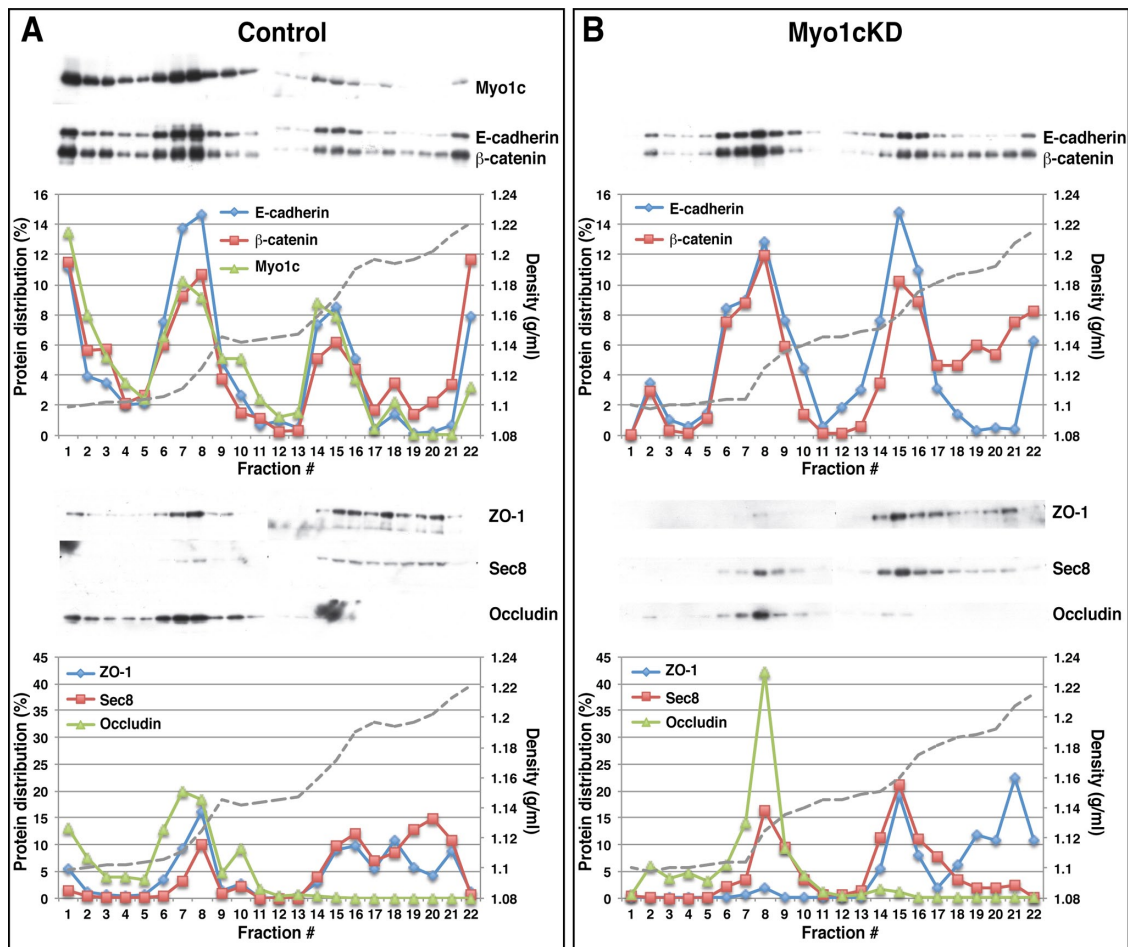


**FIGURE 6:** Fractionation of MDCK cells in iodixanol gradients. Control (A) or Myo1c-KD (B) cells were homogenized after culturing for 3 d on polycarbonate filters. Postnuclear supernatants were adjusted to 30% (wt/vol) iodixanol, overlaid with 20 and 10% iodixanol, left to stand at 4°C for 3 h, and centrifuged at  $150,000 \times g$  for 3 h. The presence of Myo1c, E-cadherin,  $\beta$ -catenin, ZO-1, Sec8, and occludin in gradient fractions was assayed by SDS-PAGE followed by immunoblotting with specific antibodies. Protein levels were quantified using ImageJ software. Densities of each fraction were calculated after measuring refractive indices with a refractometer and are plotted as dotted lines on each graph with values (in g/ml) indicated on the right y-axis.

unaffected by Myo1c KD (Figure 7E), suggesting that Myo1c does not regulate actin-filament dynamics at cell-cell contacts. We confirmed that the actin-stabilizing drug jasplakinolide reduces the mobile fraction of actin to <50%, as reported previously (Yamada *et al.*, 2005; Figure 7E). When an MDCK cell monolayer was treated with 0.2  $\mu$ M jasplakinolide, GFP-Myo1c photobleached at cell-cell contacts had the same rate of recovery and percentage mobile fraction as untreated cells (Figure 7E). Overall these findings suggest that targeting of Myo1c and actin might be regulated by independent mechanisms.

### Myo1c controls E-cadherin distribution in confluent MDCK cells

The difference in the distribution of E-cadherin in control versus Myo1c-KD cells suggests that Myo1c mediates E-cadherin trafficking by affecting its exocytosis, endocytosis, or recycling. To investigate the molecular mechanism, first we measured the amount of E-cadherin exposed to the cell surface as an indication of whether Myo1c affects E-cadherin exocytosis. When surface proteins were biotinylated, captured on streptavidin beads, and blotted for E-cadherin, no reproducible differences were detected between control

and Myo1c-KD cells (Figure 8A). These data demonstrate that there is little or no change in the amount of E-cadherin at the cell surface at steady state as a result of Myo1c KD.

In confluent MDCK cells E-cadherin was localized mostly at the lateral plasma membrane, but small amounts were detected in punctae close to the cell surface. This internal pool of E-cadherin is believed to be a result of endocytosis from the cell surface (Le *et al.*, 1999). To determine whether Myo1c regulates endocytosis of E-cadherin, we incubated cells at 18°C for 2 h, fixed them, and immunodetected E-cadherin. At 18°C vesicle recycling is blocked, and endocytosed proteins accumulate in early or sorting endosomes (Czekay *et al.*, 1997). The 18°C temperature block did not affect cell morphology or cell-cell contacts, as shown by the pattern of F-actin staining, nor was there a detectable change in the cell surface staining of E-cadherin (Figure 8B); however, there was more vesicular staining of E-cadherin in Myo1c-KD versus control cells (Figure 8B). Vesicular structures were also partially stained with anti-E-cadherin antibody in cells expressing GFP-Myo1c (Figure 8C). Although the majority of E-cadherin exists on the lateral plasma membrane, Myo1c KD may affect a small pool of E-cadherin internalized from the cell surface. Thus

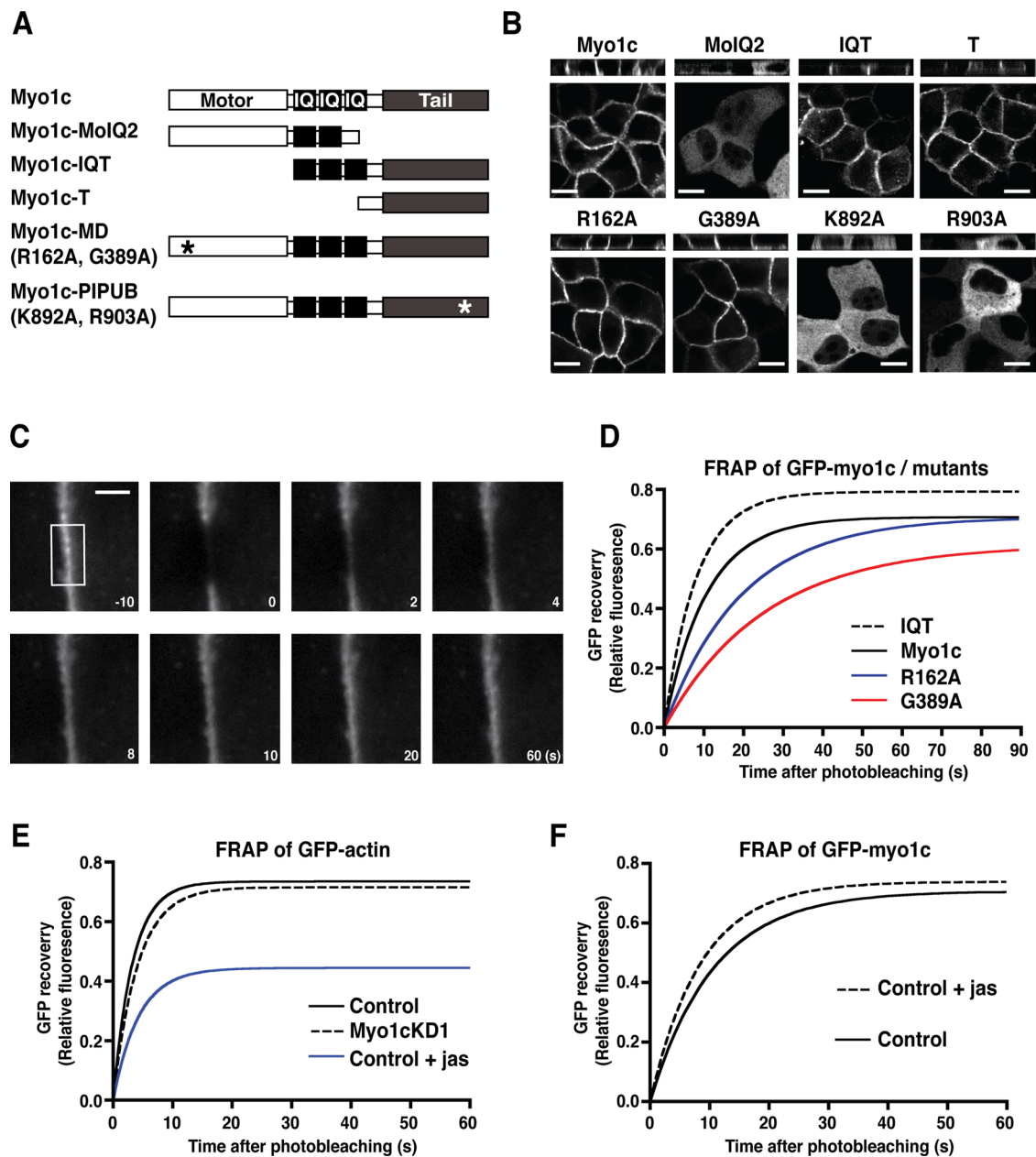


**FIGURE 7:** Myo1c domains responsible for its localization and stability at cell–cell adhesions and relation to F-actin. (A) Schematic diagram of Myo1c constructs used in this study. (B) MDCK cells transfected with GFP-Myo1c constructs as indicated were plated at high density for 3 d, fixed, and then imaged. Scale bars, 10  $\mu$ m. (C) Dynamics of GFP-Myo1c wild type and mutants were measured in live confluent MDCK monolayers using FRAP. Regions within the junctions between two adjacent transfected cells were selected for bleaching (white box in C), and the average intensity was monitored during recovery. Scale bar, 5  $\mu$ m. (D) FRAP recovery is represented by fitted curves of GFP fluorescence for GFP-Myo1c ( $n = 12$ ), GFP-IQT ( $n = 10$ ), GFP-R162A ( $n = 13$ ), and GFP-G389A ( $n = 15$ ). Average fluorescence intensity profiles ( $\pm$ SEM) are shown in Supplemental Figure S3. (E) Cell–cell contacts of Myo1c-KD cells expressing GFP-actin ( $n = 10$ ) or control cells expressing GFP-actin treated with ( $n = 10$ ) or without ( $n = 9$ ) 0.2 M jasplakinolide were photobleached, and the recovery of FRAP was analyzed as in D. (F) Jasplakinolide did not affect mobility of GFP-Myo1c.

Myo1c might affect endocytosis or stabilize E-cadherin at cell–cell adhesions.

#### Myo1c KD increases lateral movement of E-cadherin within the membrane

In addition to the translocation of E-cadherin between the plasma membrane and cytosol during trafficking, the formation of stable adherens junctions involves the movement of E-cadherin molecules

engaged in transmembrane clusters with those that are laterally diffusing in the membrane (Brieher *et al.*, 1996; Adams *et al.*, 1998; Sako *et al.*, 1998; Klingelhofer *et al.*, 2002). Translocation of E-cadherin between the plasma membrane and cytosol during trafficking and its lateral movement within the membrane (Perez *et al.*, 2008) contribute to E-cadherin dynamics. To investigate the effect of Myo1c KD on the lateral movement of E-cadherin within the membrane, we used an assay with photoactivatable green fluorescence

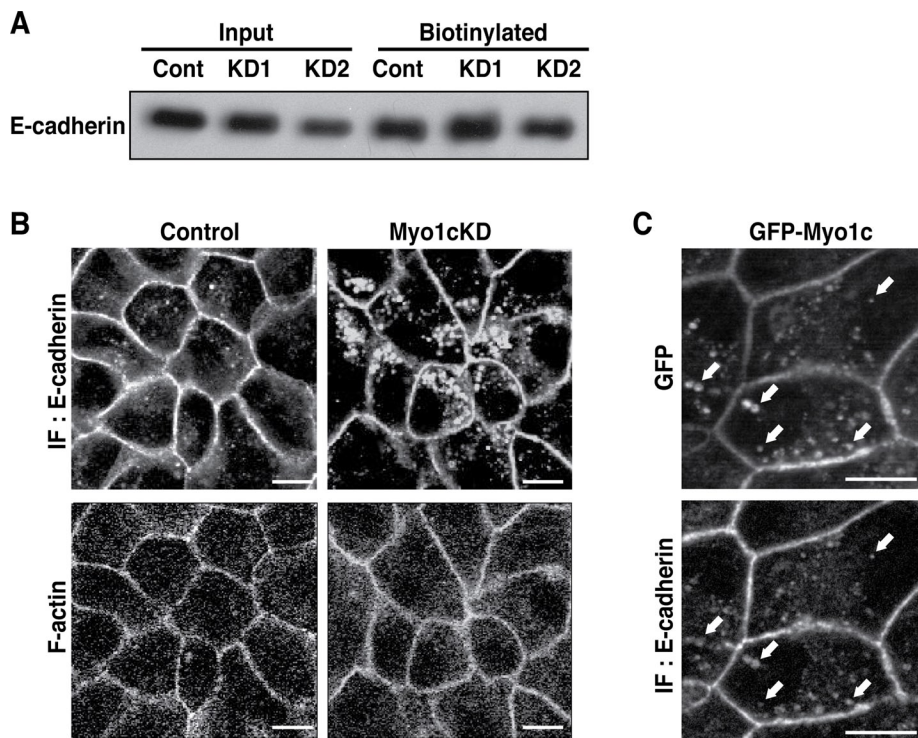


**FIGURE 8:** Myo1c KD increases the internalization of E-cadherin from cell–cell adhesions. (A) Well-polarized MDCK cells were treated with the nonpermeable biotin linker sulfo-NHS-SS-biotin, and the biotinylated proteins were captured onto streptavidin-agarose beads and detected by immunoblotting. (B) Cells cultured at high density were placed at 18°C for 2 h and fixed, and the localization of E-cadherin was detected by immunofluorescence microscopy, with F-actin identified by phalloidin staining. (C) High magnification of cells expressing GFP-Myo1c treated as in B. Vesicular structures labeled with GFP and stained with anti-E-cadherin antibody were found in cytoplasmic regions. Scale bars, 10  $\mu$ m.

protein (PAGFP) fused to E-cadherin (Canel *et al.*, 2010). As a control, we used PAGFP-Farn2Palm, which localizes to the plasma membrane through a farnesylated and doubly palmitoylated membrane targeting sequence and diffuses freely in the membrane (Konig *et al.*, 2008; Canel *et al.*, 2010). Before activation, PAGFP-E-cadherin and PAGFP-Farn2Palm were predominantly localized at the plasma membrane in confluent monolayers of control and Myo1c-KD cells (Figure 9A). After photoactivation, PAGFP-Farn2Palm diffused laterally within the membrane with the same rate in both control and Myo1c-KD cells (Figure 9, A and B; and average intensity  $\pm$  SD from 25 cells is shown in Figure S4, A and B). These results suggest that Myo1c KD does not globally affect membrane dynamics at cell–cell contacts. On the other hand, E-cadherin movement within the membrane in Myo1c-KD cells was considerably faster than in control cells (Figure S4, A and B, and Figure 9A). This observation was confirmed by calculating the average rate constant after fitting the decay curves (control, 0.0044  $s^{-1}$ ; Myo1c KD, 0.0036  $s^{-1}$ ; Figure 9B). The laterally mobile fraction of activated PAGFP-E-cadherin in Myo1c-KD cells was larger than that in control cells, as determined by comparing the reduction in fluorescence intensity from preactivation (100%) to plateau (Figure 9B; control, 53  $\pm$  6%; Myo1c KD, 30  $\pm$  14%). These results indicate that Myo1c reduces the lateral movement of E-cadherin within the membrane. This stabilization of E-cadherin might strengthen AJs.

#### Only wild-type Myo1c rescues the Myo1c KD phenotype

To evaluate the specificity of Myo1c for the KD phenotype and to test the effects of mutations in Myo1c on cell–cell contact, we

performed rescue experiments using GFP constructs. The expression level of GFP-Myo1c was almost the same as that of endogenous Myo1c, as determined by immunoblotting with anti-Myo1c antibody (Figure 10A). GFP-tagged mouse Myo1c (refractory to shRNA) expressed in Myo1c-KD cells clustered in small islands when cultured at low density, with clearly detectable cell–cell adhesions especially visible in z-sections (Figure 10B), as shown in control cells (Figure 3A). On the other hand, cells expressing GFP-Myo1cIQT, GFP-Myo1cG389A, and GFP-Myo1cK903A showed the same morphology as Myo1c-KD cells. Thus only wild-type Myo1c restored the Myo1c-KD phenotype. The studies indicate that normal motor function and PIP<sub>2</sub> binding are critical for formation of E-cadherin-mediated cell–cell adhesions.

#### DISCUSSION

Our studies show that Myo1c is a key regulator of E-cadherin targeting to cell–cell adhesion sites. At low density, Myo1c-KD cells lose their epithelial morphology due to a lack of proper E-cadherin targeting to cell–cell adhesion sites; expression of KD-resistant GFP-Myo1c restores the phenotype. Localization of E-cadherin at AJs is mediated by at least three mechanisms: exocytosis, endocytosis, and recycling (Chen *et al.*, 1999). Using mature MDCK monolayers under normal culture conditions, we could not detect

reproducible differences in extracellular targeting of E-cadherin between control and Myo1c-KD cells using biotinylation assays. One possibility is that small changes in the amount of E-cadherin at the cell surface as a consequence of Myo1c KD were not observed because biotinylation detects a relatively small subset of the total E-cadherin present at the surface in stable monolayers. Of interest, under the same high-density culture conditions, decreasing the Ca<sup>2+</sup> concentration caused a dramatic difference between control and Myo1c-KD cells: more disruption of cell–cell adhesions occurred in Myo1c-KD cells at low Ca<sup>2+</sup> concentrations than control cells. It was reported that depletion of extracellular Ca<sup>2+</sup> induces internalization of E-cadherin, which disrupts epithelial cohesion in confluent MDCK cells (Le *et al.*, 1999), and the endocytosed E-cadherin is recycled to AJs to restore cell–cell contact after changing back to normal Ca<sup>2+</sup> concentration. From this evidence, it is plausible that Myo1c KD increases the rate of E-cadherin endocytosis or decreases its recycling in low-Ca<sup>2+</sup> conditions.

In adipocytes, Myo1c facilitates GLUT4 trafficking to the plasma membrane via the exocyst (Chen *et al.*, 2007). E-cadherin is also targeted to the plasma membrane by exocytosis (Chen *et al.*, 1999; Miranda *et al.*, 2003); therefore we initially assumed that Myo1c would promote E-cadherin transport by affecting exocytosis. Plasma membrane fractionation assays, however, showed quite different fractionation patterns between Myo1c and one component of the exocyst complex, Sec8, with little effect on the fractionation pattern of Sec8 in Myo1c-KD cells. Moreover, we were unable to detect any association of Myo1c with Sec8 by coimmunoprecipitation (data not shown), even when we used the cell-permeable cross-linker

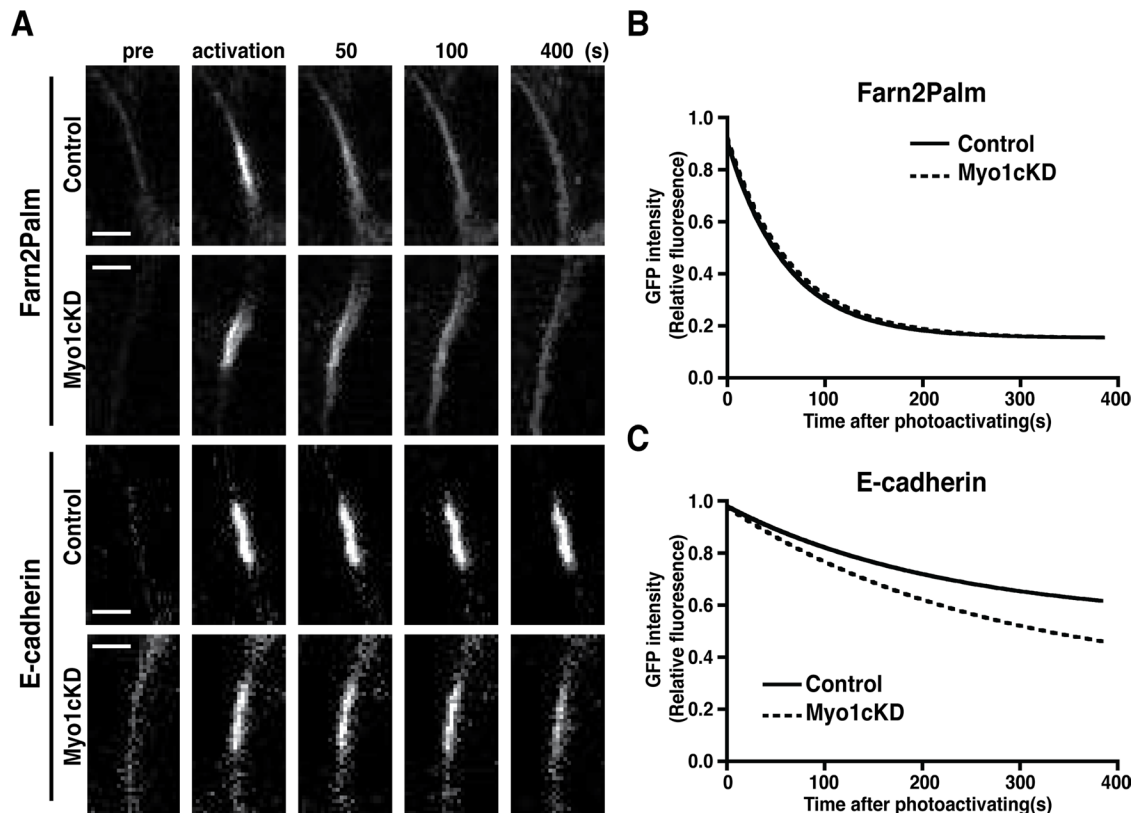


**FIGURE 9:** Myo1c KD increases the lateral movement of E-cadherin within the membrane. (A) Representative time-lapse images of PAGFP-FarnsPalm (top) and PAGFP-E-cadherin (bottom) at the plasma membrane captured preactivation (pre) and after activation in control cells and Myo1c-KD cells. Bars, 5  $\mu$ m. (B) Fluorescence decay curves after photoactivation of PAGFP-FarnsPalm and (C) PAGFP-E-cadherin. These curves are fitted to the average of GFP intensities shown in Supplemental Figure S4.

dithiobis(succinimidyl)propionate, although others successfully precipitated Myo1c with anti-Sec8 antibody (Chen *et al.*, 2007). These data therefore identify a new, exocytosis-independent function of Myo1c for targeting molecules to the plasma membrane. We also could not detect binding of Myo1c to E-cadherin,  $\beta$ -catenin, or ZO-1 with coimmunoprecipitation assays, suggesting that either the mechanism does not involve direct association of Myo1c with AJ proteins or the association is not strong enough to be detected by this method. One possibility is that Myo1c affects the class I myosin Myo1d, which interacts with  $\beta$ -catenin to regulate DE-cadherin in *Drosophila* (Petzoldt *et al.*, 2012).

Recently Myo1c was identified as a lipid raft-associated protein that is specifically involved in recycling of glycosylphosphatidylinositol (GPI)-linked cargo proteins and their delivery to the cell surface (Brandstaetter *et al.*, 2012). Myo1c-depleted cells show that GPI-linked raft markers are trapped in a perinuclear recycling compartment. Thus it is also possible that E-cadherin is targeted to lipid rafts by Myo1c; however, in contrast to T-cadherin, E-cadherin is not a GPI-linked protein (Koller and Ranscht, 1996).

In cultured adipocytes Myo1c is concentrated beneath PIP<sub>2</sub>-rich plasma membrane patches, where cortical F-actin is also abundant (Huang *et al.*, 2004). These data support our finding that targeting of Myo1c to cell-cell adhesions might depend on PIP<sub>2</sub> binding through its tail domain, because the basolateral plasma membrane is a PIP<sub>2</sub>-rich region in polarized epithelial cells. Motor domain-deleted or motor-dead mutants localize to cell-cell adhesion sites properly, and thus targeting of Myo1c to these sites is solely

dependent on PIP<sub>2</sub> binding. Of interest, after targeting to cell-cell contacts, Myo1c stability at this site is partially regulated by F-actin association according to results from the FRAP experiments with motor-deleted or motor-dead Myo1c constructs, but Myo1c itself does not affect F-actin stability at cell-cell adhesion sites because the rate of fluorescence recovery after photobleaching of GFP-actin was the same in control and Myo1c-KD cells. From this evidence, we speculate that Myo1c connects the plasma membrane to the actin cytoskeleton, which in turn stabilizes E-cadherin at cell-cell adhesion sites and facilitates clustering at nascent junctions. The mechanisms by which F-actin controls E-cadherin-based adhesions are under debate. The traditional paradigm proposes that E-cadherin- $\beta$ -catenin- $\alpha$ -catenin complexes are directly linked to F-actin through  $\alpha$ -catenin; however, recent studies suggest that  $\alpha$ -catenin assembled into cadherin-catenin complexes does not bind to actin (Yamada *et al.*, 2005). We also confirmed that membrane-associated actin is highly dynamic and that the mobility of Myo1c at cell-cell contacts is more similar to that of actin and actin-binding proteins than membrane-bound cadherin-catenin complexes. Remarkably, disrupting actin organization did not affect Myo1c dynamics, just as FRAP of E-cadherin and  $\alpha$ -catenin did not change after treatment with cytochalasin D or jasplakinolide (Yamada *et al.*, 2005). These results suggest that Myo1c shares properties intermediate to those of actin-binding proteins and cadherin-catenin complexes at cell-cell contacts.

Instead of cadherin-catenin complexes directly binding F-actin,  $\alpha$ -catenin recruits vinculin to AJs through force-dependent changes

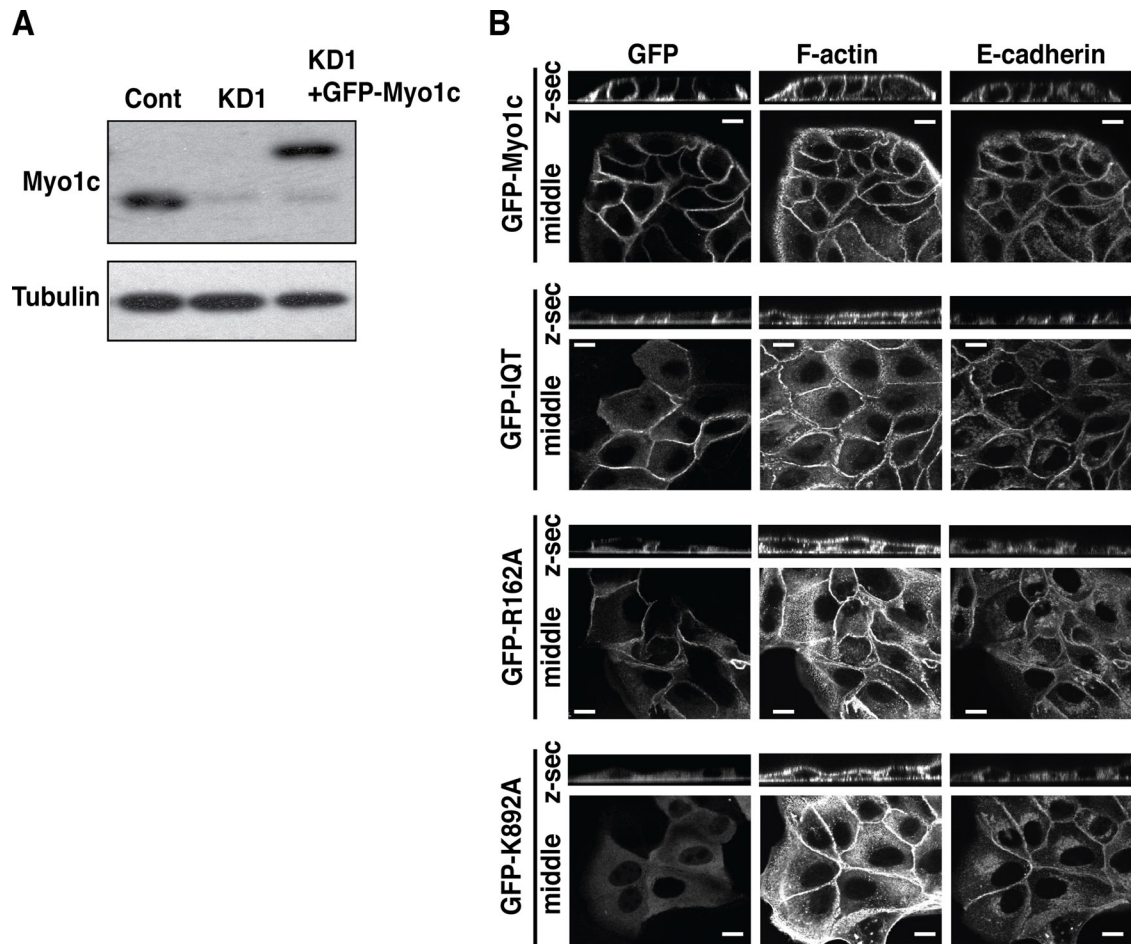


**FIGURE 10:** Reexpression of wild-type Myo1c rescues defects in adherens junction structure. (A) Immunoblot analysis of transfected MDCK cells with anti-Myo1c antibody. Equal protein concentrations were loaded and normalized using tubulin detected with anti-tubulin antibodies. (B) Myo1cKD1 cells expressing GFP-Myo1c wild type and mutants were plated at low density and then fixed and stained for E-cadherin and F-actin. Scale bars, 10  $\mu$ m. Only wild-type Myo1c rescues the phenotype.

in the conformation of  $\alpha$ -catenin (Yonemura *et al.*, 2010). EPLIN also fills the gap between  $\alpha$ -catenin and F-actin at AJs (Laakso *et al.*, 2008). Interactions between cadherin–catenin complexes and the underlying actin cytoskeleton in cells might be very dynamic and fine-tuned. It is possible that Myo1c regulates these dynamic and fine-tuned interactions at cell–cell contacts by mediating the interaction of the actin cytoskeleton with the membrane.

As reported previously, photoactivation analysis of PAGFP–E-cadherin at cell–cell adhesions clearly shows its lateral movement within the plasma membrane (Canel *et al.*, 2010). Of interest, we find that lateral movement of both PAGFP–E-cadherin and the control PAGFP–Farn2Palm is much slower than previously observed (E-cadherin:  $t_{1/2} = 188 \pm 14$  vs.  $43 \pm 4$  s; PAGFP–Farn2Palm:  $t_{1/2} = 42 \pm 2$  vs.  $15 \pm 2$  s). In addition, the remaining fluorescence intensity of PAGFP–E-cadherin plateaus at  $\sim 50\%$ , higher than the 20% previously observed. These differences might be accounted for by the differences in cell types. It is plausible that MDCK cells are more highly polarized, with more stable AJs than A431 cells. Our results from photoactivation analysis suggest that Myo1c stabilizes E-cadherin from lateral movement within the plasma membrane. Thus the reduction in E-cadherin stability as a consequence of Myo1c KD might be responsible for the higher rate of E-cadherin endocytosis at 18°C (Figure 8), higher sensitivity to lower  $\text{Ca}^{2+}$  concentrations

(Figure 5), and decreased attachment of cells to the E-cadherin extracellular domain (Figure 4).

In conclusion, our studies provide novel insights into the mechanism regulating E-cadherin dynamics by implicating Myo1c in two different aspects: Myo1c regulates both endocytosis of E-cadherin and its lateral movement within the membrane. These two mechanisms might govern simultaneously by affecting each other for fine-tuning of E-cadherin function at AJs.

## MATERIALS AND METHODS

### Plasmid construction

Oligonucleotides targeting canine Myo1c RNA and designed to contain 9–base pair hairpin loops were annealed and cloned into the *BglIII/HindIII* sites of pSUPER (OligoEngine, Seattle, WA). Sequences of the primers were as follows: Myo1cKD1 sense primer, 5′-GATCCCC**GGACACAATCAAGCACCATCC**TTCAAGAGAGGATGGTGCTTGATTGTGTCCTTTTTA-3′; Myo1cKD1 antisense primer, 5′-AGCTTAAAAAGGACACAATCAAGCACCATCC**TCTCTTGAAGGATGGTGCTTGATTGTGTCCGGG**-3′; Myo1cKD2 sense primer, 5′-GATCCCC**GCGTACCAGTGGTGAATAC**TTCAAGAGAGTATTCACCACTGGTACCGCTTTTTTA-3′; and Myo1cKD2 antisense primer, 5′-AGCTTAAAAAG**GCGTACCAGTGGTGAATAC**TCTCTTGAAGTATTCACCACTGGTACCGCGGG-3′. Bold letters

indicate Myo1c mRNA-targeting sequences; italics indicate the hairpin loops.

pEGFP-Myo1c, which includes cDNA encoding the entire open reading frame of mouse Myo1c transcript variant 2, was obtained from T. Friedman (National Institute of Deafness and Other Communication Disorders, National Institutes of Health, Bethesda, MD). To generate pEGFP-Myo1c-MoIQ2, cDNA encoding the first 754 amino acids, which includes the motor domain and first two IQ motifs, was cut from pEGFP-Myo1c by *XhoI* and *Sall* and subcloned into the *Sall* site in pEGFP-C1 (Clontech, Mountain View, CA). The sequence from the first coiled-coil region to the C-terminus (IQ1, amino acid residues 690–1028) was amplified by PCR and subcloned into the *BamHI* site in pEGFP-C1 (pEGFP-Myo1c-IQ1). To produce pEGFP-Myo1c-T, cDNA encoding amino acids 755–1028 of the tail region was cut from pEGFP-Myo1c by *Sall* and *BamHI* and subcloned into the *XhoI* and *BamHI* sites in pEGFP-C1. We made two types of motor-dead constructs, one in switch I (R162A) and one in switch II (G389A), by site-directed mutagenesis (Kunkel, 1985; Kunkel *et al.*, 1987) of pEGFP-Myo1c. In addition, we used the same mutations of basic residues in the signature motif of the PH domain that inhibit binding to PIP<sub>2</sub> and localization within membrane ruffles (K892A or R903A; Hokanson *et al.*, 2006) and refer to them as PIP<sub>2</sub>-unbinding (UB) mutants (Myo1c-PIPUB-K892A or R903A).

### Antibodies

Primary antibodies used in this study were as follows: rabbit polyclonal antibody against Myo1c (Atlas Antibodies/Sigma-Aldrich, St. Louis, MO); mouse monoclonal antibody (mAb) against the cytoplasmic domain of E-cadherin (BD Transduction Laboratories, Lexington, KY); mouse mAb for  $\beta$ -catenin (BD Transduction Laboratories); mouse mAb for Sec8 (BD Transduction Laboratories); mouse mAb against human ZO-1 (Invitrogen, Carlsbad, CA); mouse mAb against human occludin (Invitrogen); and mouse mAb for  $\alpha$ -tubulin (Sigma-Aldrich). Secondary antibodies were species-specific antibodies conjugated with Alexa Fluor 488, 564, or Cy5 (Invitrogen) for immunofluorescence microscopy or with horseradish peroxidase (Bio-Rad, Hercules, CA) for immunoblotting.

### Cell culture and transfection

MDCK-II cells (American Type Culture Collection, Manassas, VA) were cultured in DMEM supplemented with 10% fetal bovine serum. Transient transfections were done in suspension by electroporation with a Neon transfection system (Invitrogen) according to the manufacturer's instructions. At 16 h after transfection, cells were trypsinized and replated on fibronectin (FN) for the indicated times.

### Immunofluorescence microscopy and image analysis

Cells cultured on coverslips coated with 10  $\mu$ g/ml FN were fixed with 1:1 acetone/methanol for 5 min on ice and then incubated with 5% bovine serum albumin in phosphate-buffered saline for 60 min at room temperature. After the antibodies were diluted with blocking solution, the cells were incubated at 4°C overnight with primary antibody and for 30 min with secondary antibody. For actin staining, Alexa Fluor phalloidin (Invitrogen) was added to the secondary antibody. Specimens were observed at room temperature using a Leica TCS SP5 laser scanning confocal microscope (Leica, Wetzlar, Germany) equipped with an HCX PL APO lambda blue (63 $\times$ /1.40 numerical aperture) oil-immersion objective and analyzed with its associated Leica Application Suite Advanced Fluorescence software for appropriate binning of pixels and exposure time. The images were processed using Photoshop 7.0 (Adobe, San Jose, CA).

Quantitative analysis of E-cadherin at contacts (Figure S2 and Figure 5, E–G) was performed in ImageJ (National Institutes of Health, Bethesda, MD) using the line scan function. The Plot Profile feature of ImageJ was used to record the pixel intensities along a line 63 pixels in length placed perpendicular to randomly selected cell–cell contacts, and the results were saved in text format. The process was repeated for 24 contacts derived from three independent experiments. The data for each profile were then imported into Prism 5 (GraphPad Software, La Jolla, CA). Pixel intensity of background regions in the images was typically nonzero and was corrected for by subtracting a constant value from each of the intensity profiles. This led to each profile being approximately Gaussian in shape, with the tails approaching zero. Using Prism 5, we fitted a Gaussian curve to each intensity profile and recorded the SD of the fitted curve. The full-width at half-maximum (FWHM) was then calculated for each curve as the SD multiplied by 2.3548. For a given experiment, the mean and the SD of the FWHM were calculated. Similarly, the mean and SD of the maximum heights of the fitted curves were calculated.

### FRAP assay

FRAP experiments were performed using a UltraVIEW-ERS spinning disk confocal microscope (PerkinElmer, Waltham, MA) with a 60 $\times$  ApoTIRF 1.49 oil differential interference contrast objective lens controlled by Volocity (ImproVision, PerkinElmer) software. Time-lapse images of cells were taken in phenol red-free DMEM (Sigma-Aldrich) with 10% FBS and 25 mM 4-(2-hydroxyethyl)-1-piperazineethanesulfonic acid over a period of ~10 min at 37°C in a temperature-controlled chamber. Effective photobleaching was achieved using 100% 488-nm laser power. Images were analyzed using Volocity software. Time-lapse images were obtained by sequential epifluorescent and phase illumination with 0.3-s intervals and 100- to 300-ms exposure times, depending on the time-lapse interval and level of fluorescence.

### Photoactivation analysis

Photoactivation experiments were performed using a Zeiss LSM 710 confocal microscope with a plan apochromatic 40 $\times$  oil objective lens (Carl Zeiss, Jena, Germany). MDCK cells transfected with either pPAGFP-E-cadherin or pPAGFP-Farn2Palm were plated onto glass-bottom dishes and cultured 2 d after reaching confluence. Cells were maintained at 37°C and 5% CO<sub>2</sub> in a temperature- and CO<sub>2</sub>-controlled chamber. Photoactivation was achieved with a one-frame activation pulse using the lowest power of the two-photon laser needed to activate PAGFP and optimize the imaging parameters, ensuring that the signal did not saturate the detector. Activated GFP images were captured every 5 s for 80 frames with a 512  $\times$  512 pixel scan field and 4 $\times$  average. Fluorescence intensity measurements derived from the region of interest were averaged in ImageJ and exported into Prism 5 for exponential curve fitting.

### Fractionation of cell–cell adhesion complexes in iodixanol gradients

Control or Myo1c-KD cells were homogenized after culturing for 3 d on polycarbonate filters. Postnuclear supernatants were subjected to iodixanol density gradients using a modification of a previously described method (Vogelmann and Nelson, 2007). The discontinuous gradients were equilibrated at 4°C for 3 h before spinning at 150,000  $\times$  g for 3 h in a SW41Ti rotor instead of a VTi 65.1 rotor, which was unavailable.

## Other procedures

E-cadherin binding assays (Qin *et al.*, 2005), cell surface biotinylation (Le *et al.*, 1999), and immunoblotting (Tokuo and Ikebe, 2004) were performed as previously described.

## ACKNOWLEDGMENTS

We thank T. Friedman for providing the plasmid pEGFP-Myo1c, I. Macara (University of Virginia, Charlottesville, VA) for the pSUPER-luciferase vector, B. Gumbiner (University of Virginia) for the recombinant ectodomain of human E-cadherin fused to the Fc region of immunoglobulin G, and V. Brunton (Edinburgh Cancer Research Centre, Edinburgh, United Kingdom) for the pPAGFP-E-cadherin and pPAGFP-Farn2Palm. The work was supported by National Institutes of Health Grants DC009887 to H.T. and DC008793 to L.M.C.

## REFERENCES

- Adams CL, Chen YT, Smith SJ, Nelson WJ (1998). Mechanisms of epithelial cell-cell adhesion and cell compaction revealed by high-resolution tracking of E-cadherin-green fluorescent protein. *J Cell Biol* 142, 1105–1119.
- Almagro S *et al.* (2010). The motor protein myosin-X transports VE-cadherin along filopodia to allow the formation of early endothelial cell-cell contacts. *Mol Cell Biol* 30, 1703–1717.
- Applewhite DA, Barzik M, Kojima S, Svitkina TM, Gertler FB, Borisy GG (2007). Ena/Vasp proteins have an anti-capping independent function in filopodia formation. *Mol Biol Cell* 18, 2579–2591.
- Arif E, Wagner MC, Johnstone DB, Wong HN, George B, Pruthi PA, Lazzara MJ, Nihalani D (2011). Motor protein Myo1c is a podocyte protein that facilitates the transport of slit diaphragm protein Nep1 to the podocyte membrane. *Mol Cell Biol* 31, 2134–2150.
- Au JS, Puri C, Ihrke G, Kendrick-Jones J, Buss F (2007). Myosin VI is required for sorting of Ap-1b-dependent cargo to the basolateral domain in polarized MDCK Cells. *J Cell Biol* 177, 103–114.
- Balish MF, Moeller EF3rd, Coluccio LM (1999). Overlapping distribution of the 130- and 110-aDa myosin I isoforms on rat liver membranes. *Arch Biochem Biophys* 370, 285–293.
- Batters C, Arthur CP, Lin A, Porter J, Geeves MA, Milligan RA, Molloy JE, Coluccio LM (2004a). Myo1c is designed for the adaptation response in the inner ear. *EMBO J* 23, 1433–1440.
- Batters C, Wallace MI, Coluccio LM, Molloy JE (2004b). A model of stereocilia adaptation based on single molecule mechanical studies of myosin I. *Phil Trans R Soc B* 359, 1895–1905.
- Bershadsky A (2004). Magic touch: how does cell-cell adhesion trigger actin assembly? *Trends Cell Biol* 14, 589–593.
- Bose A, Guilherme A, Robida SI, Nicoloso SM, Zhou QL, Jiang ZY, Pomerleau DP, Czech MP (2002). Glucose transporter recycling in response to insulin is facilitated by myosin Myo1c. *Nature* 420, 821–824.
- Bose A, Robida S, Furcinitti PS, Chawla A, Fogarty K, Corvera S, Czech MP (2004). Unconventional myosin Myo1c promotes membrane fusion in a regulated exocytic pathway. *Mol Cell Biol* 24, 5447–5458.
- Boyd-White J, Srirangam A, Goheen MP, Wagner MC (2001). Ischemia disrupts myosin I beta in renal tubules. *Am J Physiol Cell Physiol* 281, C1326–C1335.
- Braga VM, Del Maschio A, Machesky L, Dejana E (1999). Regulation of cadherin function by Rho and Rac: modulation by junction maturation and cellular context. *Mol Biol Cell* 10, 9–22.
- Brandstaetter H, Kendrick-Jones J, Buss F (2012). Myo1c regulates lipid raft recycling to control cell spreading, migration and *Salmonella* invasion. *J Cell Sci* 125, 1991–2003.
- Brieher WM, Yap AS, Gumbiner BM (1996). Lateral dimerization is required for the homophilic binding activity of C-cadherin. *J Cell Biol* 135, 487–496.
- Canel M, Serrels A, Anderson KI, Frame MC, Brunton VG (2010). Use of photoactivation and photobleaching to monitor the dynamic regulation of E-cadherin at the plasma membrane. *Cell Adh Migr* 4, 491–501.
- Cavey M, Lecuit T (2009). Molecular bases of cell-cell junctions stability and dynamics. *Cold Spring Harb Perspect Biol* 1, a002998.
- Cavey M, Rauzi M, Lenne PF, Lecuit T (2008). A two-tiered mechanism for stabilization and immobilization of E-cadherin. *Nature* 453, 751–756.
- Chen XW, Leto D, Chiang SH, Wang Q, Saltiel AR (2007). Activation of Rala is required for insulin-stimulated Glut4 trafficking to the plasma membrane via the exocyst and the motor protein Myo1c. *Dev Cell* 13, 391–404.
- Chen YT, Stewart DB, Nelson WJ (1999). Coupling assembly of the E-cadherin/beta-catenin complex to efficient endoplasmic reticulum exit and basal-lateral membrane targeting of E-cadherin in polarized MDCK cells. *J Cell Biol* 144, 687–699.
- Coluccio LM (2008). Myosin I. *Proteins Cell Regul* 7, 95–124.
- Conti MA, Even-Ram S, Liu C, Yamada KM, Adelstein RS (2004). Defects in cell adhesion and the visceral endoderm following ablation of nonmuscle myosin heavy chain II-a in mice. *J Biol Chem* 279, 41263–41266.
- Czekay RP, Orlando RA, Woodward L, Lundstrom M, Farquhar MG (1997). Endocytic trafficking of megalin/Rap complexes: dissociation of the complexes in late endosomes. *Mol Biol Cell* 8, 517–532.
- Delva E, Kowalczyk AP (2009). Regulation of cadherin trafficking. *Traffic* 10, 259–267.
- Drees F, Pokutta S, Yamada S, Nelson WJ, Weis WI (2005). Alpha-catenin is a molecular switch that binds E-cadherin-beta-catenin and regulates actin-filament assembly. *Cell* 123, 903–915.
- Farquhar MG, Palade GE (1963). Junctional complexes in various epithelia. *J Cell Biol* 17, 375–412.
- Geeves MA, Perreault-Micale C, Coluccio LM (2000). Kinetic analyses of a truncated mammalian myosin i suggest a novel isomerization event preceding nucleotide binding. *J Biol Chem* 275, 21624–21630.
- Geisbrecht ER, Montell DJ (2002). Myosin VI is required for E-cadherin-mediated border cell migration. *Nat Cell Biol* 4, 616–620.
- Gillespie PG, Müller U (2009). Mechanotransduction by hair cells: models, molecules, and mechanics. *Cell* 139, 33–44.
- Greenberg MJ, Lin T, Goldman YE, Shuman H, Ostap EM (2012). Myosin IC generates power over a range of loads via a new tension-sensing mechanism. *Proc Natl Acad Sci USA* 109, E2433–E2440.
- Harris TJ, Tepass U (2010). Adherens junctions: from molecules to morphogenesis. *Nat Rev Mol Cell Biol* 11, 502–514.
- Hirono M, Denis CS, Richardson GP, Gillespie PG (2004). Hair cells require phosphatidylinositol 4,5-bisphosphate for mechanical transduction and adaptation. *Neuron* 44, 309–320.
- Hokanson DE, Laakso JM, Lin T, Sept D, Ostap EM (2006). Myo1c binds phosphoinositides through a putative pleckstrin homology domain. *Mol Biol Cell* 17, 4856–4865.
- Hokanson DE, Ostap EM (2006). Myo1c binds tightly and specifically to phosphatidylinositol 4,5-bisphosphate and inositol 1,4,5-trisphosphate. *Proc Natl Acad Sci USA* 103, 3118–3123.
- Huang S, Lifshitz L, Patki-Kamath V, Tuft R, Fogarty K, Czech MP (2004). Phosphatidylinositol-4,5-bisphosphate-rich plasma membrane patches organize active zones of endocytosis and ruffling in cultured adipocytes. *Mol Cell Biol* 24, 9102–9123.
- Ivanov AI, Hunt D, Utech M, Nusrat A, Parkos CA (2005). Differential roles for actin polymerization and a myosin II motor in assembly of the epithelial apical junctional complex. *Mol Biol Cell* 16, 2636–2650.
- Kambara T, Rhodes TE, Ikebe R, Yamada M, White HD, Ikebe M (1999). Functional significance of the conserved residues in the flexible hinge region of the myosin motor domain. *J Biol Chem* 274, 16400–16406.
- Kametani Y, Takeichi M (2007). Basal-to-apical cadherin flow at cell junctions. *Nat Cell Biol* 9, 92–98.
- Klingelhofer J, Laur OY, Troyanovsky RB, Troyanovsky SM (2002). Dynamic interplay between adhesive and lateral E-cadherin dimers. *Mol Cell Biol* 22, 7449–7458.
- Koller E, Ranscht B (1996). Differential targeting of T- and N-cadherin in polarized epithelial cells. *J Biol Chem* 271, 30061–30067.
- Konig I, Schwarz JP, Anderson KI (2008). Fluorescence lifetime imaging: association of cortical actin with a Pip3-rich membrane compartment. *Eur J Cell Biol* 87, 735–741.
- Kunkel TA (1985). Rapid and efficient site-specific mutagenesis without phenotypic selection. *Proc Natl Acad Sci USA* 82, 488–492.
- Kunkel TA, Roberts JD, Zakour RA (1987). Rapid and efficient site-specific mutagenesis without phenotypic selection. *Methods Enzymol* 154, 367–382.
- Laakso JM, Lewis JH, Shuman H, Ostap EM (2008). Myosin I can act as a molecular force sensor. *Science* 321, 133–136.
- Le TL, Yap AS, Stow JL (1999). Recycling of E-cadherin: a potential mechanism for regulating cadherin dynamics. *J Cell Biol* 146, 219–232.
- Li XD, Rhodes TE, Ikebe R, Kambara T, White HD, Ikebe M (1998). Effects of mutations in the gamma-phosphate binding site of myosin on its motor function. *J Biol Chem* 273, 27404–27411.
- Maddugoda MP, Crampton MS, Shewan AM, Yap AS (2007). Myosin VI and vinculin cooperate during the morphogenesis of cadherin cell cell contacts in mammalian epithelial cells. *J Cell Biol* 178, 529–540.

- Miranda KC, Joseph SR, Yap AS, Teasdale RD, Stow JL (2003). Contextual binding of P120ctn to E-cadherin at the basolateral plasma membrane in polarized epithelia. *J Biol Chem* 278, 43480–43488.
- Mostov KE, Verges M, Altschuler Y (2000). Membrane traffic in polarized epithelial cells. *Curr Opin Cell Biol* 12, 483–490.
- Nambiar R, McConnell RE, Tyska MJ (2009). Control of cell membrane tension by myosin-I. *Proc Natl Acad Sci USA* 106, 11972–11977.
- Nelson WJ (2009). Remodeling epithelial cell organization: transitions between front-rear and apical-basal polarity. *Cold Spring Harb Perspect Biol* 1, a000513.
- Perez TD, Tamada M, Sheetz MP, Nelson WJ (2008). Immediate-early signaling induced by E-cadherin engagement and adhesion. *J Biol Chem* 283, 5014–5022.
- Petzoldt AG, Coutelis JB, Geminard C, Speder P, Suzanne M, Cerezo D, Noselli S (2012). DE-cadherin regulates unconventional myosin Id and myosin Ic in *Drosophila* left-right asymmetry establishment. *Development* 139, 1874–1884.
- Poupon V, Stewart A, Gray SR, Piper RC, Luzio JP (2003). The role of Myosin 18p in clustering, fusion, and intracellular localization of late endocytic organelles. *Mol Biol Cell* 14, 4015–4027.
- Qin Y, Capaldo C, Gumbiner BM, Macara IG (2005). The mammalian scribble polarity protein regulates epithelial cell adhesion and migration through E-cadherin. *J Cell Biol* 171, 1061–1071.
- Ruppert C, Godel J, Müller RT, Kroschewski R, Reinhard J, Bähler M (1995). Localization of the rat myosin I molecules Myr 1 and Myr 2 and in vivo targeting of their tail domains. *J Cell Sci* 108, 3775–3786.
- Sako Y, Nagafuchi A, Tsukita S, Takeichi M, Kusumi A (1998). Cytoplasmic regulation of the movement of E-cadherin on the free cell surface as studied by optical tweezers and single particle tracking: corralling and tethering by the membrane skeleton. *J Cell Biol* 140, 1227–1240.
- Sasaki N, Shimada T, Sutoh K (1998). Mutational analysis of the switch II loop of *Dictyostelium* myosin II. *J Biol Chem* 273, 20334–20340.
- Shen L, Weber CR, Turner JR (2008). The tight junction protein complex undergoes rapid and continuous molecular remodeling at steady state. *J Cell Biol* 181, 683–695.
- Shewan AM, Maddugoda M, Kraemer A, Stehbens SJ, Verma S, Kovacs EM, Yap AS (2005). Myosin 2 is a key Rho kinase target necessary for the local concentration of E-cadherin at cell-cell contacts. *Mol Biol Cell* 16, 4531–4542.
- Shimada T, Sasaki N, Ohkura R, Sutoh K (1997). Alanine scanning mutagenesis of the switch I region in the atpase site of *Dictyostelium discoideum* myosin II. *Biochemistry* 36, 14037–14043.
- Smutny M, Cox HL, Leerberg JM, Kovacs EM, Conti MA, Ferguson C, Hamilton NA, Parton RG, Adelstein RS, Yap AS (2010). Myosin II isoforms identify distinct functional modules that support integrity of the epithelial zonula adherens. *Nat Cell Biol* 12, 696–702.
- Speder P, Adam G, Noselli S (2006). Type Id unconventional myosin controls left-right asymmetry in *Drosophila*. *Nature* 440, 803–807.
- Tokuo H, Ikebe M (2004). Myosin X transports Mena/Vasp to the tip of filopodia. *Biochem Biophys Res Commun* 319, 214–220.
- Tuxworth RI, Weber I, Wessels D, Addicks GC, Soll DR, Gerisch G, Titus MA (2001). A role for myosin VII in dynamic cell adhesion. *Curr Biol* 11, 318–329.
- Vasioukhin V, Bauer C, Yin M, Fuchs E (2000). Directed actin polymerization is the driving force for epithelial cell-cell adhesion. *Cell* 100, 209–219.
- Vogelmann R, Nelson WJ (2007). Separation of cell-cell adhesion complexes by differential centrifugation. *Methods Mol Biol* 370, 11–22.
- Wagner MC, Barylko B, Albanesi JP (1992). Tissue distribution and subcellular localization of mammalian myosin I. *J Cell Biol* 119, 163–170.
- Wagner MC, Blazer-Yost BL, Boyd-White J, Srirangam A, Pennington J, Bennett S (2005). Expression of the unconventional myosin Myo1c alters sodium transport in M1 collecting ducts cells. *Am J Physiol* 289, C120–C129.
- Wagner MC, Molitoris BA (1997). ATP depletion alters myosin I beta cellular location in Llc-Pk1 Cells. *Am J Physiol* 272, C1680–C1690.
- Walmsley SJ, Broeckling C, Hess A, Prenni J, Curthoys NP (2010). Proteomic analysis of brush-border membrane vesicles isolated from purified proximal convoluted tubules. *Am J Physiol Renal Physiol* 298, F1323–F1331.
- Yamada S, Pokutta S, Drees F, Weis WI, Nelson WJ (2005). Deconstructing the cadherin-catenin-actin complex. *Cell* 123, 889–901.
- Yeaman C (2003). Ultracentrifugation-based approaches to study regulation of Sec6/8 (exocyst) complex function during development of epithelial cell polarity. *Methods* 30, 198–206.
- Yonemura S, Wada Y, Watanabe T, Nagafuchi A, Shibata M (2010). Alpha-catenin as a tension transducer that induces adherens junction development. *Nat Cell Biol* 12, 533–542.